Available online at www.sciencedirect.com
ScienceDirect
Cement and Concrete Research 36 (2006) 1635–1642
Cement and Concrete Research

Addition of cement to lime-based mortars: Effect on pore structure and vapor transport

M.J. Mosquera [a,*], B. Silva [b], B. Prieto [b], E. Ruiz-Herrera [a]

[a] Departamento de Química-Física, Facultad de Ciencias, Universidad de Cádiz, 11510 Puerto Real, Spain
[b] Departamento de Edafología, Facultad de Farmacia, Universidad de Santiago de Compostela, 15706 Santiago de Compostela, Spain

Received 23 January 2004; accepted 13 October 2004

Abstract

The main focus of this work is to determine the effect of cement addition, a common practice in many restorations, on the pore structure of lime-based mortars. A second target is to establish correlations between microstructure and water vapor transport across the mortar, which is a key characteristic of building decay. In order to achieve these objectives, we prepared a set of mortars consisting of air-hardening lime with a progressively increasing cement content, as well as a mortar containing hydraulic lime. Several different techniques, most notably mercury intrusion porosimetry and scanning electron microscopy in the backscatter mode, were used to investigate the pore structure. The results from these procedures led to the conclusion that porosity and pore size are progressively reduced as cement content increases. Moreover, an excellent correlation between pore radius parameter and the vapor diffusion coefficient was established. Hydraulic lime mortar exhibited textural parameters and diffusivity values halfway between those of the different lime/cement mixes studied.

Keywords: Microstructure-B; Transport properties-C; $Ca(OH)_2$-D; Mortar-E; Restoration

1. Introduction

Lime-based mortars were commonly used in building until the second half of the 19th century, when they started to be replaced by a new binder, namely portland cement. Numerous inconveniences regarding the application of lime mortar, including long setting and hardening times, weak mechanical properties, and low internal cohesion [1], certainly promoted this substitution. However, the application of cement mortars in the restoration of historic buildings has had numerous adverse effects because the cement-based mixes are too hard, rigid, and impermeable. In general, mortars should be more permeable to vapor transport than the other masonry materials used so that water, which contains damaging ions, can evaporate before it spreads throughout the structure. Also, pointing mortars in particular must be considerably weaker than the rest of the masonry to accommodate slight movements of the building. Moreover, in addition to these drawbacks, cement exhibits other adverse properties; for example, it has a much higher thermal expansion coefficient than most masonry and it can contain soluble salts that leach out over time [1,2]. Recent work has thus focused on the development of new mortars for restoration work that meet the aforementioned requirements [3–5].

The revival of lime as a restoration binder has also spawned numerous studies which attempt to achieve a complete characterization of lime-based mortar technology [1,6]. Still, there is surprisingly little reliable information as to the manner in which processing variables such as constituents or mixing ratios influence the final properties of the product, which, in turn, play a relevant role in the success of restoration. Obviously, the lack of knowledge concerning lime technology is the main stumbling block to achieving a standardized application. In fact, in many present restorations, a low cement content is added to

* Corresponding author. Tel.: +34 956 016331; fax: +34 956 016288.
E-mail address: mariajesus.mosquera@uca.es (M.J. Mosquera).

0008-8846/$ - see front matter © 2005 Elsevier Ltd. All rights reserved.
doi:10.1016/j.cemconres.2004.10.041

lime-based mixes in order to minimize inconveniences, such as long hardening and setting times. The purpose of this paper is thus to evaluate the effect of cement on the microstructure of lime-based mortars. The second target of this study is to establish a relationship between the resulting changes in the pore structure and water vapor transport through the mortar, which is relevant to building decay. The additional characterization of mortar containing hydraulic lime as a binder delimits the potential of this material as an alternative to aerial lime.

2. Experimental

2.1. Mortars

Lime mortars containing only air-hardening lime as a binder were compared with three mixes in which lime was partially replaced by cement. In addition, a mortar containing hydraulic lime as a binder was also tested. Before the preparation of the mortars, the selected materials were subjected to tests as follows: Mineralogical analysis of binders and aggregate was carried out by means of X-ray diffraction (Fig. 1) whereas the soluble ions of the selected aggregate were analyzed by means of atomic absorption and emission spectrophotometry. In addition, a granulometry analysis was performed on the selected aggregate (Table 1).

The aggregate used was quartz sand of high purity, as made evident by its diffraction pattern (Fig. 1a). Its low soluble salt content (below 0.2% wt) guaranteed its suitability as a component of the mortars. Granulometry values are given in Table 1, which shows that the aggregate diameter ranged mainly from 0.5 to 2 mm.

The binders used were portland cement containing interground fly ash of type CEM II/B-V32.5 (according to the standard UNE-ENV 197-1 [7]) and hydraulic lime of type NHL 3.5 (according to the standard UNE-ENV 459-1 [8]), both of which are readily available as commercial products. Air-hardening lime was prepared in the laboratory from commercial calcium oxide of type CL90 (according to the standard UNE-ENV 459-1 [8]) with the traditional method of slaking under continuous stirring. Water at laboratory temperature and with low soluble ions content was used in a ratio of limewater of 1:1. After 1 year of aging in water, the lime was then used to prepare the various mortars. The diffraction pattern corresponding to the lime after slaking (Fig. 1b) shows the success of this process as portlandite is the main component. The hydraulic lime (Fig. 1c) used contained portlandite, calcite, and, in minor proportion, some silicates. The pattern found for the cement (Fig. 1d) shows the diffractogram typical of this material. The chemical composition of the three binders used in this work, which were supplied directly by the manufacturers, is shown in Table 2.

The mortars were prepared in accordance with the standard UNE-EN 1015-4 [9]. The aggregate–binder ratio

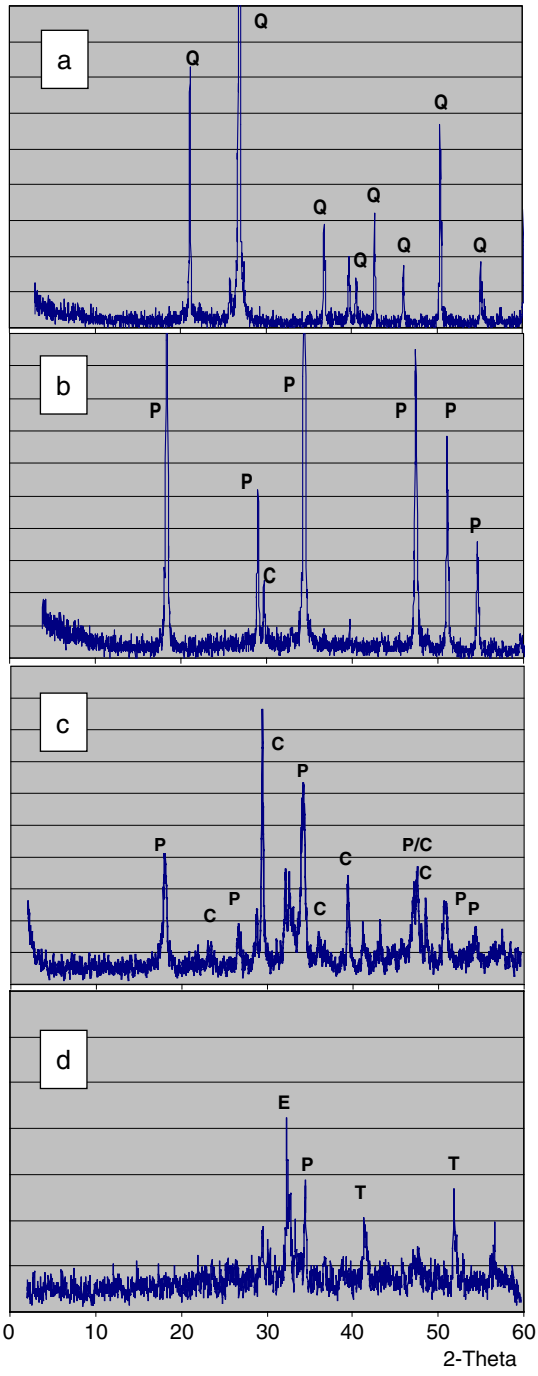

Fig. 1. X-ray diffraction patterns. (a) Aggregate. (b) Aerial lime after slaking. (c) Hydraulic lime. (d) Cement. (Q: quartz; P: portlandite; C: calcite; E: ettringite; T: tombermorite).

(by volume) was 3:1. Table 3 shows details of the mixes evaluated. In order to achieve a suitable workability, a different amount of water was added to each of the mixes. As is shown in Table 3, the aerial lime mix did not require addition of water. The mortars were prepared as 4×4×16 cm prisms, except those specimens used in the water vapor diffusivity test, which required the preparation of 5×5×2 cm specimens (see Section 2.3). As commercial casts with these dimensions are not available, they were built in the

Table 1
Percentage by weight corresponding to sand granulometry fractions (mm)

>4	4–2	2–1	1–0.5	0.5–0.25	0.25–0.1	0.1–0.05	<0.05
0.13	10.51	25.29	19.17	14.61	10.23	6.41	13.62

laboratory. All mortars were maintained in the molds for 72 h, except the aerial lime mortar, which was demolded after a suitable consistency was achieved 7 days later. Finally, the specimens were cured under laboratory conditions (20 °C and 60% RH). We had originally intended to allow the curing phase to continue until carbonation had been completed. Thus, in order to control the carbonation process, the specimens were regularly subjected to the phenolphthalein test. It was suitable for aerial lime mortars but not for the others in which the positive result of the test (purple color) may be due to the presence of others hydroxides apart from $Ca(OH)_2$. Thus, carbonation was monitored also by X-ray analysis chartering the increase in the calcite/portlandite ratio.

The carbonation can be a slow process, as is well documented [1] it can extend over years. We decided thus to stop curing after 6 months. In this time, the mixes containing aerial lime exhibited a high carbonation percentage while carbonation in the mixes with hydraulic lime had already been completed in this period. The results reported in this work were all taken as an average value of three similar specimens. The coefficients of variation were below 10%.

2.2. Pore structure

The main tool for characterizing textural properties was Mercury Intrusion Porosimetry (MIP). However, since the use of this technique on cement-based materials has been called into doubt [10–14], we used additional procedures, such as scanning electron microscopy and water saturation tests to validate porosimetry results. These experimental procedures were carried out as follows:

- Mercury Intrusion Porosimetry (MIP): The measurements were carried out with a Pascal Porosimeter (Fision Instruments Milan, Italy) over a pressure range between 10^{-3} and 400 MPa. By assuming a contact angle of 130° and a mercury surface tension of 484×10^{-3} N/m, the pore radii ranging from 78 μm to 10^{-3} μm were characterized. Specimens with an average volume of 2 cm^3 were cut from the mortar prisms using low speed sawing. Before being tested, specimens were cleaned in a microwave bath and were dried at 60 °C until a constant weight was achieved. After drying at 60°, residual water could stay trapped in the narrowest pores [14]. However, this is not a limitation in our study because our objective is to establish a comparison between pore structure and water transport properties. It is obvious that water entrapped in the specimens after drying at 60° is still present during the vapor diffusivity test.
- Scanning Electron Microscopy (SEM): Small pieces cut from the mortar specimens were impregnated with a polyester resin. The surfaces of each piece were then polished. A 435-VP Leo scanning electron microscope (Cambridge, United Kingdom) in the backscatter electron (BSE) mode was used to characterize the microstructure of the polished surfaces. The low backscatter coefficient of polyester resin permitted a clear distinction of the porous space.
- Optical Microscopy (OM): An *Optiphot-Pol* Nikon Optical Microscopy with reflected light (Tokyo, Japan) was used to visualize the same polished specimens, as a previous phase to the SEM study.
- Open Porosity Test: the porosity accessible to water was determined by means of a hydrostatic scale following the RILEM procedure [15].
- Picnometer Test: The real density of the mortar powders was determined using a picnometer, according to the standard UNE-EN 1936 [16]. From the real density value and the bulk density value which was calculated from mass and volume data, a total porosity value was obtained. The difference between this value and the previously calculated open porosity is the so-called closed porosity, which corresponds to the porous space into which water cannot enter.

2.3. Vapor transport

Water vapor transport was investigated by means of an automatic set-up developed in our laboratory. The device, which is based on the standard cup test [17–19], is a modification of an earlier moisture absorption-measuring apparatus [20]. Specific details about the device are

Table 2
Chemical composition of binders (% wt)

Component	CaO	$Ca(OH)_2$	$CaCO_3$	SiO_2	MgO	CO_2	Al_2O_3	Fe_2O_3	SO_3	K_2O	Na_2O	Others**
A Lime	94.5	–	–	0.40*	0.60	1	0.2*		–	–	–	–
H Lime	57.0	26.0	21	19	0.92	–	1.6	0.45	0.6	0.16	0.06	0.38
Cement	47.8	–	–	27	2.4	–	9.8	5.3	2.4	1.8	0.2	

A is aerial; H is hydraulic. *Maximum content. **TiO_2, MnO, SrO and Cr_2O_3.

Table 3
Composition of mortars

Mix	Ratio (by volume)	Water/solid ratio (by volume)
Sand/aerial lime	3:1	–
Sand/aerial lime/cement	27:8:1	0.5
Sand/aerial lime/cement	27:6:3	1.5
Sand/aerial lime/cement	27:4.5:4.5	2.25
Sand/hydraulic lime	3:1	0.5

included in an earlier paper [4]. The experimental test was performed as follows: first, specimens were cut from 5×5×2 cm mortars as slabs 1 cm thick. After the slabs were dried at 60 °C until reaching a constant weight, they were placed as a cover on a cup made of methyl methacrylate in the shape of a cube without an upper side. A moisture saturated ambient condition (RH 98%) was maintained in the cup, the perimeters of which were sealed with silicone paste A (Panreac Química S.A., Barcelona, Spain). The cup was then placed into a gas-tight receptacle in which a stable moisture content and temperature (17 °C) were maintained. At the start of the tests, low relative moisture (3%) was achieved in the chamber by means of a desiccating agent (Silicagel; Panreac Química S.A., Barcelona, Spain). Under these conditions, the moisture gradient across the specimen promoted water vapor flux. The moisture in the chamber gradually increased until stabilizing at an RH of ca. 20%. The cup mass decrease was measured continuously with a scale interfaced to a computer, located above the climatic chamber. The monitoring of the cup mass in this fashion thus allowed the progress of vapor transport to be registered continuously and displayed in situ with the computer software. Once the relative moisture in the climatic chamber stabilized, a steady vapor flow was reached. Vapor diffusion coefficients were calculated from steady flow data.

In order to compare the diffusivity values of the mortars studied with those of stones typically used in historic buildings, the vapor transport of three stones with different textures, namely biocalcarenite, limestone, and granite, was examined. Slabs of these stones measuring 4 cm square and 1 cm thick were thus tested using the same procedure described above.

3. Results and discussion

3.1. Pore structure

Table 4 shows the intruded porosity and bulk density values obtained from the porosimetry test. The latter were gleaned from volume data, which were calculated with the porosimeter before pressurization had occurred. These values were close to those obtained from specimen dimensions (Table 5), with all variation coefficients below 7%. For mortars containing aerial lime as a binder, the progressive increase in cement content reduced the porosity from 26% to 18%, and consequently, bulk density was raised. Mortar containing hydraulic lime exhibited a significantly lower porosity than that of aerial lime mortar, with the porosity value halfway between that of the lime/cement mixes 8:1 and 6:3.

Table 4
Results from mercury porosimetry

Mix	Bulk density (g/cm^3)	Porosity (vol.%)	Maximum radius (μm)
Sand/lime* 3:1	1.949	25.75	15.25–0.15
Sand/lime/cement, 27:8:1	1.960	25.39	5.15–0.15
Sand/lime/cement, 27:6:3	2.002	21.06	0.15
Sand/lime/cement, 27:4.5:4.5	2.204	18.44	0.15
Sand/hydraulic lime	2.049	22.04	0.28

*Lime is aerial lime.

Differential pore radius distributions are shown in Fig. 2. The aerial lime mortar exhibited a bimodal distribution with the two porous volume maxima located at ca. 15 and 0.15 μm. The percentage of total porosity corresponding to each region was 52% and 48%, respectively. The addition of cement to the mix had a significant effect on the distribution. As cement content increased, the porous volume of the macropore region progressively decreased. Moreover, the threshold radius of the macropores also decreased, as can be seen in Fig. 2. The bidispersion was maintained only for the mortar containing the lowest cement content. In this mortar, the maximum for the macropores (67% of the total porosity) shifted towards a radius value of ca. 5 μm while the maximum of microporous (33% of the total porosity) had a value of 0.15 μm. In the two samples with the highest cement content, the macropore region completely disappeared so that practically all porous volume was located within a narrow range between 0.33 and 0.02 μm. The distribution of the hydraulic lime specimen was also monodisperse, with the pore radii range showing values slightly higher than those of the lime-cement mortars (1.50–0.05 μm). The value for maximum volume intruded corresponded to a radius of ca. 0.28 μm. These results indicate that cement may tend to fill up the larger pores found in lime. This would explain why the addition of

Table 5
Results from RILEM and picnometer tests

Mix	Bulk density (g/cm^3)	True density (g/cm^3)	Open porosity (vol.%)	Closed porosity (vol.%)
Sand/lime*, 3:1	1.896	2.817	26.88	5.80
Sand/lime/cement, 27:8:1	1.993	2.670	26.15	1.46
Sand/lime/cement, 27:6:3	2.009	2.730	23.16	3.22
Sand/lime/cement, 27:4.5:4.5	2.062	2.705	20.27	3.46
Sand/hydraulic lime	2.022	2.721	22.41	3.22

*Lime is aerial lime.

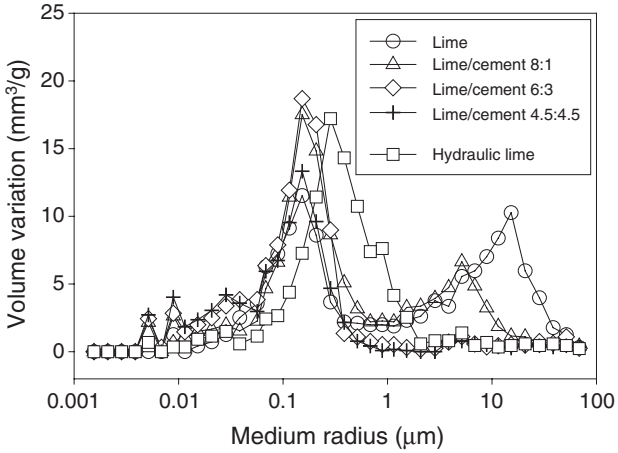

Fig. 2. Pore radius distributions. Aerial lime is referred to as lime.

cement generates a dramatic reduction in pore size in lime mortar. As for hydraulic mortar, it exhibits a microstructure similar to that of the two lime/cement mortars with the highest cement content.

Fig. 3 is a representative set of backscatter SEM views of the mortars studied. In order to show as complete an image of the microstructure as possible, we selected a small magnification. The visualization of the specimens studied by optical microscopy under reflected light showed the same pore morphology that the SEM.

Nevertheless, it is easy to see the heterogeneous nature of both pore type and pore size of the different mortars. Fig. 3a, for example, clearly shows that two classes of pore geometry coexist in lime mortar. Whereas some of the pores are spherical in form, others are elongated and both irregularly and highly convoluted in outline. Most of the spherical pores are in fact interconnected by elongated ones. Casual inspection of the pore sizes indicates that the spherical pores range in radius up to ca. 150 μm. The origin of these two kinds of porosity is clear: the spherical pores are air voids whereas the convoluted pores are cracks caused by shrinkage of the material during its drying phase.

The addition of cement (Fig. 3b) promoted a significant reduction in porous volume as well as in the pore size. The

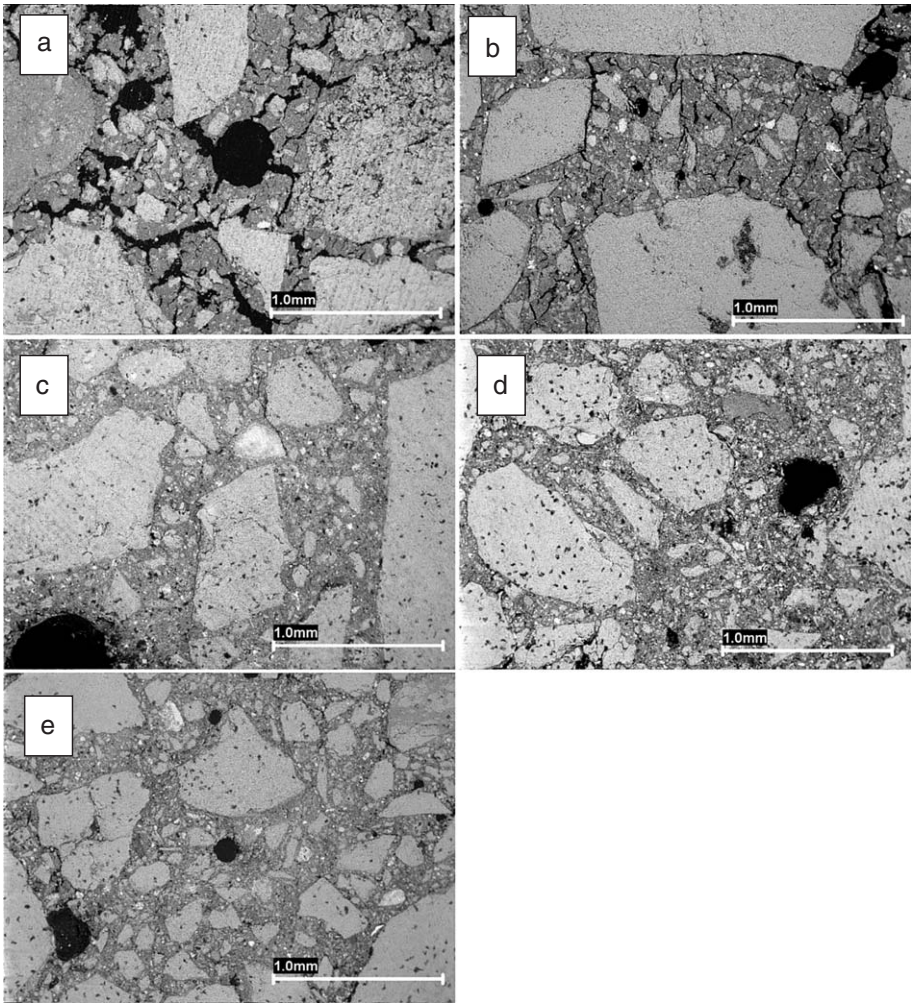

Fig. 3. Backscatter SEM images of the mortars corresponding to the binder content as follows. (a) Aerial lime. (b) Aerial lime/cement 8:1. (c) Aerial lime/cement 6:3. (d) Aerial lime/cement 4.5:4.5. (e) Hydraulic lime.

actual porous structure, however, is similar to that of lime mortar in that it contains the two different types of pores (spherical and elongated). As cement content increased, a sharp reduction in the total porous volume was observed. Interestingly, the number of elongated pores decreased sharply while decrease in the number of spherical pores was slight (see Fig. 3c and d). This fact suggests that most of the spherical pores in question are isolated without any connection. The microstructure of hydraulic lime mortar (Fig. 3e) was found to be similar to that of the latter two mixes in that isolated spherical pores predominated. These facts can be easily explained if the material strength is considered. As cement content increases, the mortar gets stronger and the cracks are fewer. The specimens with the highest cement content (Fig. 3c and d) and the hydraulic mortar (Fig. 3e) are strong enough to resist the shrinkage stresses; hence the cracks have practically disappeared. Finally, it is important to indicate that most of the spherical pores in question are isolated, without any interconnection; this is usual in the air voids typically formed in cement-based materials.

The SEM visualization permitted us to reach several conclusions about the suitability of the MIP technique for characterizing the texture of these mortars. It is obvious that the shape of the pores is quite different from the cylindrical pores assumed in the Washburn model used in the MIP procedure. Moreover, as the larger pores are interconnected by elongated ones, mercury cannot penetrate these large porous regions until the pressure is high enough to allow it to enter such narrow spaces. This porous volume is thus indiscriminately registered as entryways. In addition, some pores are actually left out of the procedure because they are larger than the upper range of measurement (78 μm) or because they are isolated pores into which mercury cannot enter. In summary, our results corroborate the conclusions presented by Diamond [10,11]: Pore size distributions from MIP data are really a better reflection of the physics of mercury intrusion than of the actual sizes of the pores present. However, it is obvious that information about mercury movement is valuable in characterizing the microstructure associated with transport. Thus, from a practical point of view, this procedure can be used to obtain valuable information concerning key parameters such as water transport. Indeed, as noted below, we were able to establish a direct relationship between the pore radius distributions as determined by means of MIP and experimental vapor diffusivity coefficients. Finally, we observed that the reduction in both pore size and total porosity in lime with increasing cement content observed with MIP was corroborated by SEM photographs. MIP is thus a suitable procedure for performing a comparative study between samples.

In the results obtained from the RILEM test (Table 5), we observed that open porosity values followed the same trend and were similar to those found by means of MIP (variation coefficient below 10%). This underscores the suitability of MIP for characterizing the accessible porosity of these specimens. The slight increase in open porosity was attributed to the different measuring ranges of both procedures. In the case of MIP, pores with radii over 78 μm cannot be detected. The noted variation may thus correspond to macropores that were quantified exclusively with the hydrostatic scale method. As for closed porosity, we observed that lime mortar exhibited a higher value than did the other mixes studied. However, for mixes containing lime and cement, the closed porosity (Table 5) increased slightly as cement content increased, although this parameter remained stable for the two specimens with the highest cement content. This trend was corroborated by SEM images. In comparison, the photograph corresponding to the lowest cement content exhibited a high connection between pores that was clearly reduced in the other mixes. Hydraulic lime mortar showed a value equal to that of lime/cement mix 6:3.

3.2. Vapor transport

The transport of water vapor due to relative moisture gradient is described by Fick's Law, according the following equation:

$$Q = D\frac{A\Delta C}{l}\cdot t \tag{1}$$

where D is vapor diffusivity (m^2/s); Q is cup mass decrease (g); l is specimen thickness (m); A is specimen area (m^2), ΔC is moisture concentration gradient (g/m^3), and t is time (s).

Thus, by plotting Ql/Ah versus time (Fig 4), vapor diffusivity values, which are shown in Table 6, were calculated directly from the slope of a linear regression of data where a steady vapor flow was attained. As noted above, this occurred when the relative moisture in the

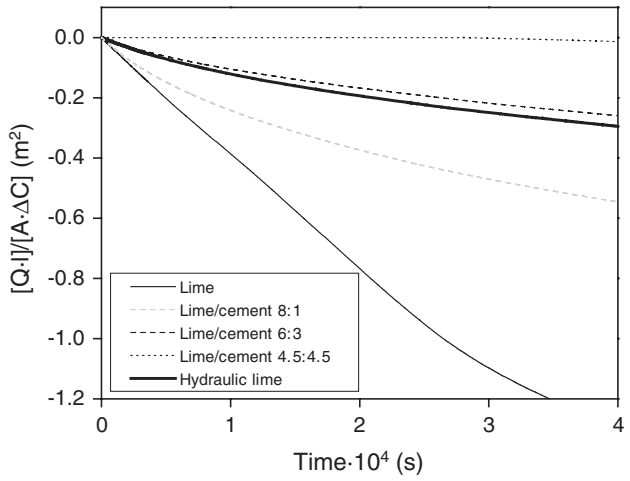

Fig. 4. Vapor transport curves. (Q: cup mass decrease (g); l: specimen thickness (m); A: specimen area (m^2); ΔC: moisture concentration gradient (g/m^3). Aerial lime is referred to as lime.

climatic chamber was stabilized. For the mortars studied, steady flow was achieved in times ranging from under 1 h (for aerial lime mortar) to 10 h (for mortar with the highest cement content). The tests were considered finished when a minimum of 3000 experimental data readings corresponding to the linear phase were obtained. This occurred in a time range from 12 h (for aerial lime mortar) to 72 h (for mortar with the highest cement content). Obviously, the high quantity of data registered (>3000) permitted a better characterization of the transport process than manual procedures, in which the number of points is often below 20. The low standard deviations obtained between replications are a good indication the reproducibility of the experiments.

The high linear correlation coefficients (r>0.995) exhibited in all the plots suggest that Fickian diffusion indeed occurs. The vapor diffusion coefficient corresponding to lime mortar was a magnitude order higher than those from the other mixes. The coefficient was found to decrease progressively as cement content increased. As previously proposed by other authors [21–23], the diffusivity variation may be explained by the decreases in porosity and pore size values. In the case of mortar containing hydraulic lime, both the diffusivity value as well as the textural parameters were halfway between those for the mix containing a lime/cement ratio of 8:1 and the mix with a ratio of 6:3. Thus, the same trend was followed here as had been found in aerial lime mortars. In order to quantify the effect of the textural parameters (porosity and pore radius) on the diffusivity, a sequential multiple regression, where textural parameters are the independent variables and diffusivity is the dependent variable, was performed.

Fig. 5 shows the response surface corresponding to the adjustment of the data. For mixes exhibiting bidispersion, the pore radius parameter was calculated as the weighted average of the two radii corresponding to the maximum volume intruded. For the monodisperse distributions, pore radius corresponded directly to the maximum volume intruded.

The stepwise multiple regression showed that porosity does not significantly (P>0.99) influence diffusivity. As seen by the form of the response surface, diffusivity is actually controlled by the pore radius parameter; thus, a good linear correlation between the two parameters was thus found (r=0.9905). Visual examination of Fig. 3 indicates

Table 6
Vapor diffusion coefficients

Mortars	Diffusivity 10^{-6} (m^2/s)	Stones	Diffusivity 10^{-6} (m^2/s)
Lime*	29.05	Biocalcarenite	0.53
Lime/cement, 8:1	5.40	Limestone	0.44
Lime/cement, 27:6:3	4.47	Granite	0.24
Lime/cement, 4.5:4.5	3.13		
Hydraulic lime	2.17		

*Lime is aerial lime.

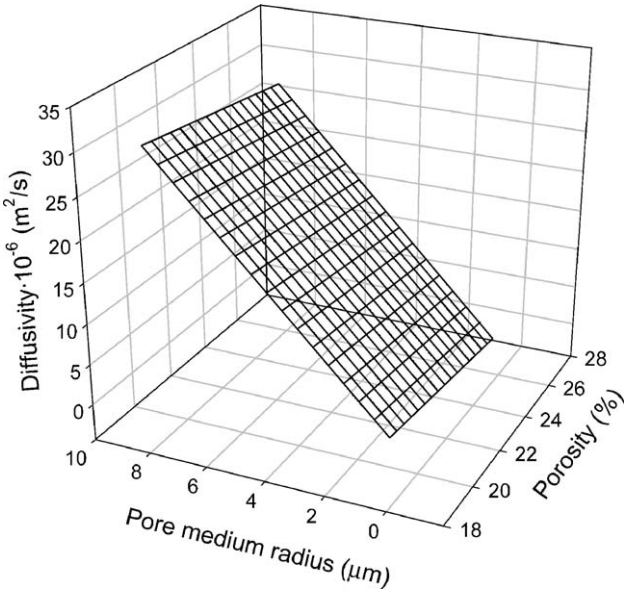

Fig. 5. Response surface corresponding to the multiple regression between the defined parameters.

that the presence of cracks in the mortar studied plays a significant role in the pore distribution. Therefore, the cracking actually controls the diffusivity parameter.

Finally, Table 6 shows diffusivity values of stones, calculated using the same procedure employed for calculating that of the mortars. In this case, the test was maintained for over 72 h, registering more than 3000 data points. Linear regression coefficients were above 0.9900. The diffusivity values of the stones were significantly lower than those obtained from the mortars, a fact which demonstrates that all the mixes studied, including those containing cement, are more permeable to water vapor than are building stones.

4. Conclusions

(1) From MIP results, we concluded that lime-based mortars reduced both their porous volume and their pore size as cement content in the mix increased. Pore structure varied from a bidisperse distribution, with two well-differentiated pore radii (15 and 0.15 μm) to a monodisperse distribution, in which the radii measurements were shifted to a sharply reduced range (0.33–0.02 μm). In this last case, the air voids are not interconnected and hence they are not quantified by MIP.

(2) Although SEM images showed pores with forms different from the classical cylindrical geometry assumed by MIP, a similar trend was observed: Accessible porosity and pore size were both reduced in line with increased cement content. In addition, microscopy showed the existence of blocked pores, which was not characterized in an obvious fashion with porosimetry.

(3) A good correlation between texture and vapor diffusivity was established. The presence of cracks, which modify substantially the pore radius distribution, was the relevant parameter in this correlation.
(4) From (1), (2), and (3), it is possible to conclude that MIP is a suitable tool for characterizing transport properties.
(5) Mortar containing hydraulic lime exhibited a pore structure and a diffusivity value that were both halfway between those corresponding to the aerial lime/cement mixes 8:1 and 6:3. Therefore, the restoration mortars which use a mix of aerial lime with a low cement content as agglomerate are more suitable than those containing hydraulic lime as a binder.
(6) Diffusivity values of the three representative stones tested were significantly lower than those from the mortars studied. We can thus conclude that the addition of cement in the proportions used here generates more permeable mixes than the typical masonry of historic buildings.

Acknowledgments

This work was supported by a contract with the company Diconsa, Diseño y Construcción S.A., which was financed by "Dirección General de I+D de la Xunta de Galicia".

References

[1] K. Elert, C. Rodriguez-Navarro, E.S. Pardo, E. Hansen, O. Cazalla, Lime mortars for the conservation of historic buildings, Stud. Conserv. 47 (2002) 62–75.
[2] K. Callebaut, J. Elsen, K. Van Balen, W. Viaene, Nineteenth century hydraulic restoration mortars in the Saint Michael's Church (Leuven, Belgium) natural hydraulic lime or cement? Cem. Concr. Res. 31 (2001) 397–403.
[3] A.P. Duffy, T.P. Cooper, S.H. Perry, Repointing mortars for conservation of a historic stone building in Trinity College, Dublin, Mat. Struct. 26 (1993) 302–306.
[4] M.J. Mosquera, D. Benítez, S.H. Perry, Pore structure in mortars applied on restoration. Effect on properties relevant to decay of granite buildings, Cem. Concr. Res. 32 (2002) 1833–1888.
[5] P.F. ÓBrien, E. Bell, S. Pavia Santamaria, P. Boyland, T.P. Cooper, Role of mortars in the decay of granite, Sci. Total Environ. 167 (1995) 103–110.
[6] R.S. Boynton, Chemistry and technology of lime and limestone, 2nd ed., John Wiley & Sons, New York, 1980.
[7] AENOR (Asociación Española de Normalización y Certificación), UNE-EN 197-1, Cemento. Parte 1: Composición, especificaciones y criterios de conformidad para los cementos comunes, 2000.
[8] AENOR (Asociación Española de Normalización y Certificación), UNE-ENV 459-1: 2002, Cales para construcción. Parte 1: Definiciones, especificaciones y criterios de conformidad, 2002.
[9] AENOR (Asociación Española de Normalización y Certificación), UNE-EN 1015-4: 1999, Método de ensayo de los morteros para albañilería. Parte 2: Toma de muestras total de morteros y preparación de morteros para ensayo, 1999.
[10] S. Diamond, Aspects of concrete porosity revisited, Cem. Concr. Res. 29 (1999) 1181–1188.
[11] S. Diamond, Mercury porosimetry. An inappropriate method for the measurement of pore size distributions in cement-based materials, Cem. Concr. Res. 30 (2000) 1517–1525.
[12] C. Gallé, Effect of dying on cement-based materials pore structure as identified by mercury porosimetry—a comparative study between oven-, vacuum-, and freeze-dying, Cem. Concr. Res. 31 (2001) 1467–1477.
[13] R. Kumar, B. Bhattacharjee, Study on some factors affecting the results in the use of MIP method in concrete research, Cem. Concr. Res. 33 (2003) 417–424.
[14] S. Diamond, A discussion of the paper "Effect of drying on cement-based materials pore structure as identified by mercury porosimetry—a comparative study between oven, vacuum and freeze-drying" by C. Gallé, Cem. Concr. Res. 33 (2003) 169–170.
[15] RILEM, Test No. I.1: Porosité accessible à Íeau. Recommended tests to measure the deterioration of stone and assess the effectiveness of treatment methods, Mat. Struct. 13 (1980) 175–253.
[16] AENOR (Asociación Española de Normalización y Certificación), UNE-EN 1936:1999, Métodos de ensayo para la piedra natural. Determinación de la densidad real y aparente y de la porosidad abierta y total, 1999.
[17] Instituto Centrale do Restauro-Commisione Normal (ICR-CNR), Doc. Normal 21/85. Alterazioni dei materiali Lapidei e Trattamenti Conservativi. Proposte per L'Unificazione dei Metodi Sperimentali di Studio e di Controlo. Permeabilita al vapor ́dacqua. Rome, Italy, 1985.
[18] ASTM E96-90, Standard test methods for water vapor transmission of materials, ASTM, Philadelphia, PA, 1990, pp. 685–695.
[19] Deutsches Institut fuer Normung, DIN 52615, Bestimmung der Wasserdampf-durchlässigkeit von Bau- und Dämmstoffen, BEUTH, Berlin, 1987.
[20] M.J. Mosquera, R. Alcántara, J. Martín, A new procedure for performance moisture absorption tests, Am. Ceram. Soc. Bull. 77 (9) (1998) 76–81.
[21] L. Bágel, V. Cívica, Relationship between pore structure and permeability of hardened cement mortars: on the choice of effective pore structure parameter, Cem. Concr. Res. 27 (8) (1997) 1225–1235.
[22] H.W. Reinhardt, K. Gaber, From pore size distribution to an equivalent pore size of cement mortar, Mat. Struct. 23 (1990) 3–15.
[23] A.S. El Dieb, R.D. Hooton, Evaluation of the Katz–Thomson model for estimating the water permeability of cement based materials from mercury intrusion porosimetry data, Cem. Concr. Res. 24 (3) (1994) 443–455.